Baryon stopping in high energy collisions in the DPMJET–III model

J. Ranft[1], R. Engel[2], and S. Roesler[3]

[1] Physics Dept. Universität Siegen, D–57068 Siegen, Germany, e–mail: Johannes.Ranft@cern.ch
[2] University of Delaware, Bartol Res. Inst., Newark DE 19716 USA, e–mail: eng@lepton.bartol.udel.edu
[3] SLAC, P.O. Box 4349, Stanford CA 94309 USA, sroesler@slac.stanford.edu

SLAC–PUB–8734

To be published in the proceedings of the meeting Monte Carlo 2000, Lisboa

A recently discovered feature of hadron production in nuclear collisions is the large stopping of the participating nucleons in hadron–nucleus and nucleus–nucleus collisions. Experimental data demonstrating this effect have been presented in [1,2].

Multistring fragmentation models like the Dual Parton Model (DPM) or similar models did originally not show this enhanced stopping in nuclear collisions. Therefore, in order to incorporate the effect into multistring fragmentation models new diquark breaking DPM–diagrams acting in hadron–nucleus and nucleus–nucleus collisions were proposed by Kharzeev [3] and Capella and Kopeliovich [4] and investigated in detail by Capella and collaborators [5,6]. Similar ideas were discussed by Vance and Gyulassy[7] and by Casado [8].

The Monte Carlo implementation into DPMJET–II.5 of the new diquark breaking diagrams of Kharzeev [3] and Capella and Kopeliovich [4] was first discussed by Ranft [9] . The implementation into DPMJET–III [10] of these diagrams differs somewhat from [9] and is described here.

There are two possibilities for the first fragmentation step of a diquark. Either we get in the first step a baryon, which contains both quarks of the diquark and the string junction or in the first step a meson is produced containing only one of the two quarks and the baryon is produced in one of the following fragmentation steps. This mechanism was implemented under the name *popcorn* fragmentation in the Lund chain fragmentation model JETSET [11,12] which is presently used in DPMJET. The popcorn mechanism alone is not enough to explain the baryon stopping observed experimentally in hadron–nucleus and nucleus–nucleus collisions [1,2].

In Ref.[9] we describe these new diquark breaking DPM–diagrams in detail. This will not be repeated here. The two important diagrams are

(i)GSQBS, the Glauber sea quark mechanism of baryon stopping, this diagram acts in nuclear collisions already at low energy.

(ii)USQBS, the unitary sea quark mechanism of baryon stopping, this mechanism leads to baryon stopping also in proton–proton collisions at collider and cosmic ray energies.

In DPMJET–III we first construct the system of parton chains according to the model without the diquark breaking diagrams. Having this we search for situations (i) as plotted on the left hand side of Fig. 1 or situations (ii) (not plotted), where the left lower diquark is replaced by an antiquark. On the left hand side in Fig. 1 we have a diquark–quark chain and a seaquark–diquark chain with the (upper) diquark and seaquark belonging to the same projectile hadron and also the (lower) diquark and valence–quark belonging to the same target–nucleon. In situation (ii) we have a diquark–quark chain and a seaquark–anti–seaquark chain with the (upper) diquark and seaquark belonging to the same projectile hadron and also the (lower) anti–seaquark and valence–quark belonging to the same target–nucleon. The chain system is transformed as plotted on the right hand side of Fig.1. The projectile diquark is split and the two resulting quarks come to the upper ends of both chains and the projectile seaquark goes into the middle of the second chain and determines the position where the baryon is produced. The sea quarks in Fig. 1 might be Glauber sea quarks or unitary sea quarks.

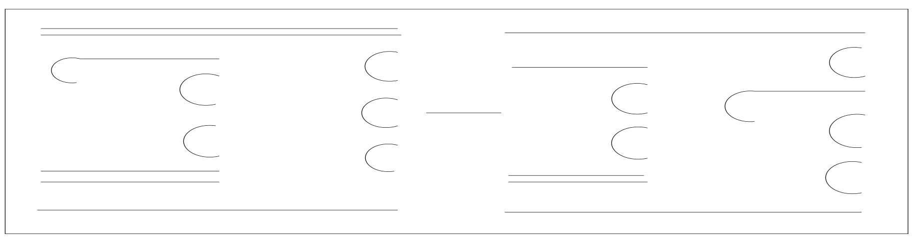

Fig. 1. Diquark breaking in an original diquark–quark and seaquark–diquark chain system.

Besides the situations already discussed we consider also the ones where projectile and target are exchanged as well as situations with anti–diquarks.

We split the diquark by sampling for one of the two resulting valence quarks (randomly choosen) a normal valence quark x_{v1} and give to the second valence quark $x_{v2} = x_d - x_{v1}$. For each of the new diquark breaking diagrams (GSQBS and USQBS) we have to introduce a new parameter. These parameters give the probability for the diquark breaking mechanisms to occur, given a suitable sea quark is available and given that the diquark breaking mechanism is kinematically allowed. For an original diquark–quark chain of small invariant mass, which originally just fragments into two hadrons, the diquark breaking is often not allowed. The optimum values of the new parameters are determined by comparing DPMJET–III with experimental data on net–baryon distributions. We obtain for the GSQBS parameters the value 0.6 and use the same value for the USQBS parameter.

Introducing the new baryon stopping mechanisms into DPMJET we get an significant modification of the model in different sectors: (i)The Feynman–x distributions of leading protons in proton–proton and proton–nucleus collisions. The leading particle production is especially important for the cosmic ray cascade simulation. (ii)The net–p ($p - \bar{p}$) and net–Λ ($\Lambda - \bar{\Lambda}$) rapidity distributions in hadron–nucleus and nucleus–nucleus collisions. These are the data on the enhanced baryon stopping mentioned already above. (iii)The production of hyperons and anti–hyperons in nuclear collisions. We present here examples for (i) and (ii).

In Fig. 2 we compare the distribution in the energy fraction x_{lab} carried by the leading proton. The data are photoproduction and DIS measurements from the HERA collider at $\sqrt{s} \approx 200$ GeV [13]. We compare to DPMJET–III for p–p collisions at $\sqrt{s} = 200$ GeV. The forward production of leading protons is not expected to depend strongly on the reaction channel. We present the DPMJET–III distributions for the models with and without the diquark breaking diagrams (No Sto in the plot). The new diagrams modify the distributions mainly at intermediate x_{Lab} values where, unfortunately, no experimental data exist at present. Therefore, further conclusions cannot be drawn at this point.

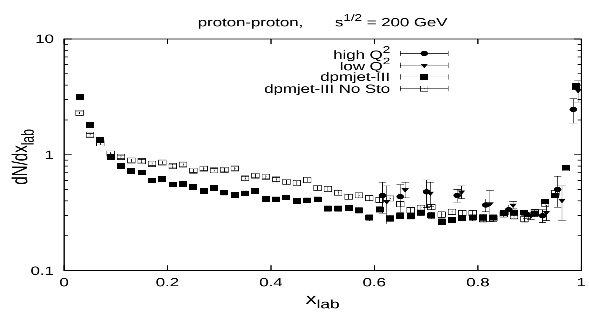

Fig. 2. Energy fraction x_{lab} carried by the leading proton. The data are photoproduction and DIS measurements at $\sqrt{s} \approx 200$ GeV [13] compared to DPMJET–III with and without (No Sto) the diquark breaking diagrams for p–p collisions at $\sqrt{s} = 200$ GeV.

In Fig. 3 we compare the net–proton distributions according to the models with and without the diquark breaking diagrams with data in p–Au collisions [2]. The dip at central rapidity, which occurs in the model without the baryon stopping diagrams is filled. The full model follows the relatively flat distribution at central rapidities shown by the data.

In Fig. 4 we compare the DPMJET–III model with and without the diquark breaking diagrams with data on net–proton production in central S–S collisions. Also here the significant dip at central rapidity in the model without the new diagrams is much less pronounced in the full model, however, the agreement to the data [2] is not perfect.

The presence of the new baryon stopping diagrams modifies also the extrapolation of multistring models to cosmic ray energies. The energy fractions

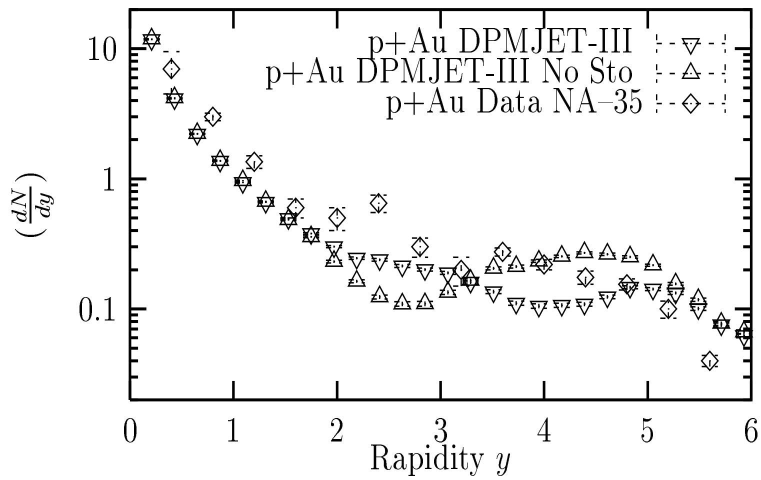

Fig. 3. Net proton ($p - \bar{p}$) rapidity distribution in p–Au collisions. The DPMJET–III results with and without (No Sto) the diquark breaking diagrams are compared with data [2].

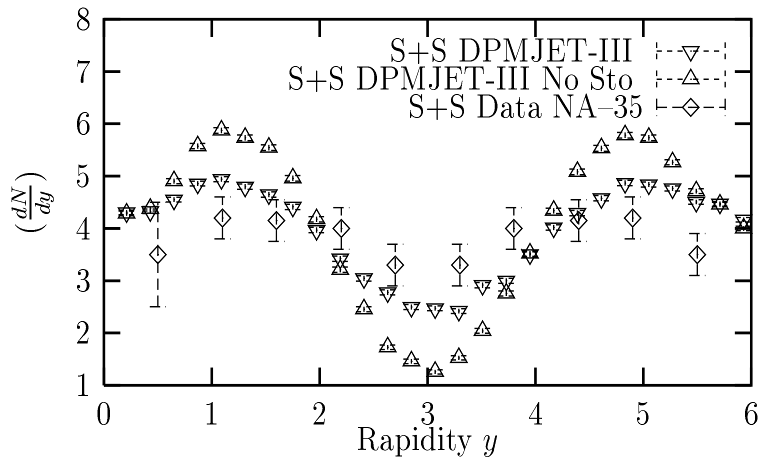

Fig. 4. Net proton ($p-\bar{p}$) rapidity distribution in central S–S collisions. The DPMJET–III results with and without (No Sto) the diquark breaking diagrams are compared with data [2].

carried by baryons decrease against those predicted by models without the new diagrams. The energy fractions carried by mesons and the spectrum weighted moments of mesons increase as compared to models without the new diagrams. We present as function of the energy for two important variables the predictions of DPMJET-III with and without the new baryon stopping diagrams. All our plots are for p–p collisions, the model behaves in a rather similar way also for p–Air collisions. We first discuss plots, where the baryon stopping mechanism causes significant differences.

The cosmic ray spectrum–weighted moments are defined as moments of x_{lab} distribution for the production of secondary particles i in hadron–hadron and hadron–nucleus collisions

$$F_i(x_{lab}) = x_{lab}\frac{dN_i}{dx_{lab}} \tag{1}$$

as follows

$$f_i = \int_0^1 (x_{lab})^{\gamma-1} F_i(x_{lab}) dx_{lab}. \tag{2}$$

Here $-\gamma \simeq -1.7$ is the power of the integral cosmic ray energy spectrum. The spectrum–weighted moments for nucleon–air collisions, as discussed in [14], determine the uncorrelated fluxes of energetic particles in the atmosphere.

We also introduce the energy fraction K_i :

$$K_i = \int_0^1 F_i(x_{lab}) dx_{lab} \tag{3}$$

As for x_{lab}, the upper limit for K is 1 in h–nucleus collisions.

In Fig.5 we present the spectrum weighted moments for charged pions in p–p collisions as function of the cms energy $\sqrt{s}$.

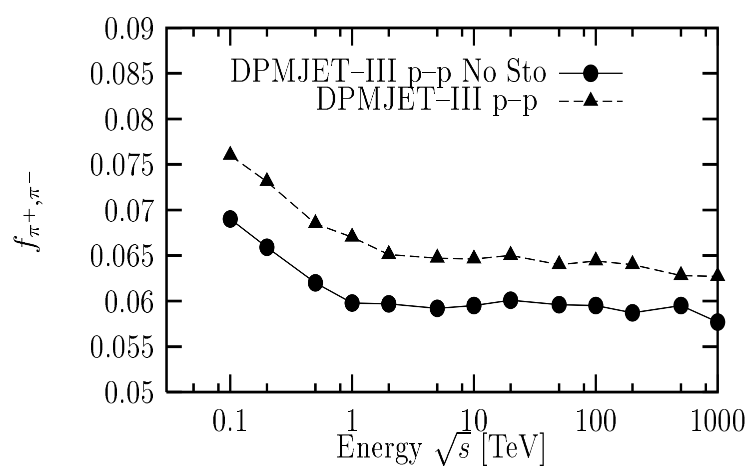

Fig. 5. Spectrum weighted moments for charged pion production in p–p collisions as function of the cms energy $\sqrt{s}$.

In Fig.6 we present again for pp collisions the energy fraction K for net baryons $B - \bar{B}$ (baryon minus antibaryon). The difference between $K_{B-\bar{B}}$ and K_B is the energy fraction going into antibaryons $K_{\bar{B}}$ which is equal to the energy fraction carried by the baryons which are newly produced in baryon–antibaryon pairs.

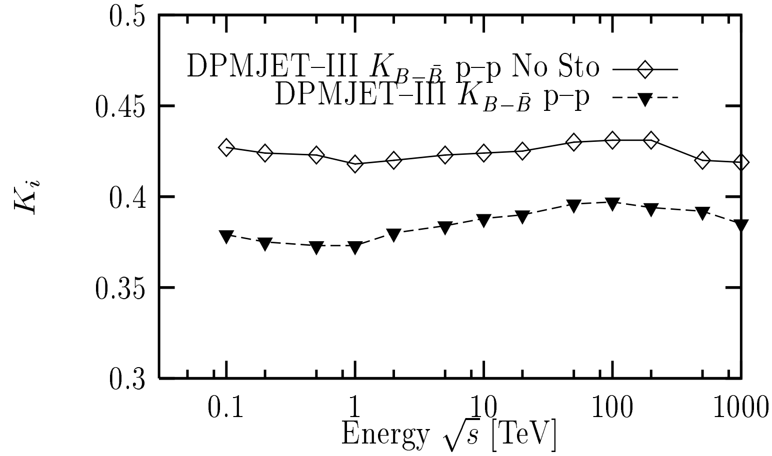

Fig. 6. Laboratory energy fractions for net baryons (baryon minus antibaryon) $B-\bar{B}$ production in p–p collisions as function of the cms energy $\sqrt{s}$.

There are also observables where the difference between the two versions of the model are rather insignificant. Examples are the average transverse momentum of charged hadrons as function of the energy and the average charged multiplicity $< n_{ch} >$ as function of the collision energy.

Acknowledgements The work of S.R and R.E. is supported by the US Department of Energy under contracts DE–AC03–76SF00515 and DE–FG02 91ER40626, respectively.

References

1. NA35 Collaboration, T. Alber et al. , *Z. Phys.* C 64(1994)195.
2. NA35 Collaboration, T. Alber et al. , *Eur. Phys. J.* C2(1998)643.
3. D. Kharzeev, *Phys.Lett.* B 378(1996)238.
4. A. Capella and B. Kopeliovich, *Phys. Lett.* B381(1996)325.
5. A. Capella, E. G. Ferreiro and C. A. Salgado, *Phys. Lett.* B459(1999)27.
6. A. Capella and C. A. Salgado, Baryon stopping and hyperon enhancement in the improved dual parton model, *hep–ph/9903414, preprint LPT Orsay 99–20* (1999).
7. S. E. Vance and M. Gyulassy, Anti–hyperon enhancement through baryon junction loops, Preprint *Cu–YP–929, nucl–th/9901009* , 1999.
8. J. A. Casado, *hep–ph/9810357v3, Manchester preprint MC–TH–98–17* (1999).
9. J. Ranft, Baryon stopping in high energy collisions and the extrapolation of hadron production models to cosmic ray energies, Preprint *hep–ph/0002137*, 2000.
10. S. Roesler, R. Engel and J. Ranft, The Monte Carlo event generator DPMJET–III, presented at the same meeting by S. Roesler.
11. T. Sjöstrand, *Comp. Phys. Comm.* 82(1994)74.
12. B. Andersson, G. Gustafson and T. Sjöstrand, *Physica Scripta* 32(1985)574.
13. A. Solano, HERA, by H1 and ZEUS Collaborations, *Nucl. Phys. Proc. Suppl.* 82(2000)36.
14. T. K. Gaisser, *Cosmic Rays and Particle Physics*, Cambridge University Press, 1990.